Die approbierte Originalversion dieser Diplom-/Masterarbeit ist in der Hauptbibliothek der Technischen Universität Wien aufgestellt und zugänglich.
http://www.ub.tuwien.ac.at

The approved original version of this diploma or master thesis is available at the main library of the Vienna University of Technology.
http://www.ub.tuwien.ac.at/eng

MASTER THESIS

Characterization of the AEgIS scintillating fiber detector FACT for antihydrogen detection

submitted by

David Haider
Puchenauer Kreuzweg 38,
A-4048 Puchenau

under supervision of

Hon.-Prof. Dipl.-Phys. Dr. Eberhard Widmann
Dipl-Ing. Dr. Chloé Malbrunot

at

Vienna University of Technology (TU Wien)
Stefan Meyer Institute for Subatomic Physics (SMI)
Austrian Academy of Science (ÖAW)

November 5, 2017

Abstract

The Antimatter Experiment: Gravity, Interferometry, Spectroscopy (AEgIS) at the Antiproton Decelerator at CERN has the goal to produce antihydrogen atoms ($\bar{H}$) at low temperatures based on positronium charge exchange. In order to detect the production of antihydrogen the products of its annihilation will be tracked by a barrel-shaped scintillating fiber detector. This master thesis deals with the characterization and preparation of this Fast Annihilation Cryogenic Tracking (FACT) detector to be ready for the first production of antihydrogen within the AEgIS apparatus this year. The thesis particularly focuses on the performance of the Multi Pixel Photon Counters (MPPCs) used in FACT to read out scintillating fibers in view of an accurate calibration of the detector. The properties of the silicon photomultipliers including a detailed analysis of their gain, their photon detection efficiency (PDE), the afterpulse probability and the overall level of dark count noise are explored at various operating parameters. The results regarding the Hamamatsu Photonics S10362-11-100C MPPC that is dominantly used in FACT are presented. From this analysis general guidelines are derived to optimize the detection efficiency for antihydrogen annihilations. This thesis also aims to document the current implementation of the detector that will be used to measure antihydrogen this year.

Kurzfassung

Das *Antimatter Experiment: Gravity, Interferometry, Spectroscopy* (AEgIS) am Antiproton Entschleuniger (AD) an der Europäische Organisation für Kernforschung (CERN) hat das Ziel, Antiwasserstoff-Atome ($\bar{\mathrm{H}}$) durch Positronium Ladungsaustausch zu erzeugen. Alle $\bar{\mathrm{H}}$-Atome, die nach ihrer Bildung in der Umgebung der Produktionszone annihilieren, können durch die Vermessung ihrer Zerfallsteilchen mit Hilfe eines Szintillationsfiber-Detektor rekonstruiert werden. Im Zuge dieser Masterarbeit wird der *Fast Annihilation Cryogenic Tracking* (FACT) Detektor charakterisiert und auf seinen Einsatz dieses Jahr bei der ersten Produktion von Antiwasserstoff innerhalb des AEgIS Experiments vorbereitet. Dabei liegt der Fokus auf die Leistung der Silizium-Photodioden, auch *Multi Pixel Photon Counters* (MPPCs) genannt, die zum Auslesen der Lichtsignale der Szintillatoren verwendet werden. Die Eigenschaften der Photodioden, wie die Höhe der Signalverstärkung, die Nachweiswahrscheinlichkeit für Photonen (PDE), die Wahrscheinlichkeit für Nachpulse und das Ausmaß der gesamten Hintergrundsignale, werden bei verschiedenen Betriebseinstellungen genau vermessen. Zwei Modelle von Silizium-Photodioden von Hamamatsu Photonics (S10362-11-100C und S12571-100C) sind in FACT verbaut und die Ergebnisse deren Charakterisierung werden präsentiert. Aus diesen Messungen werden generelle Richtwerte ermittelt mit denen die Nachweisrate für Antiwasserstoff-Annihilationen erhöht werden kann. Als Grundlage zu diesen Nachforschungen ist der aktuelle Status des Detektors dokumentiert.

Acknowledgment

Throughout my studies I have had the support of many encouraging people. They have made my time at the university a wonderful period of my life and without them it would not have been possible for me to complete this thesis in the form it has today. In the following, I would like to say thank you to all who have accompanied me on my way and highlight those who made it a particular effort to help me finish this work.

First of them all are my loving parents Christine and Karl and my wonderful girlfriend Clara with their endless support for my studies. They guided me when I had doubts and gave me the energy to keep going.
Furthermore, I would like to thank Chloé Malbrunot, who was my immediate supervisor when I worked at CERN, for all the valuable input on the problems I encountered. She made an effort to read though many versions of this thesis and helped me to improve it with an inexhaustible amount of suggestions.
Moreover, I am very grateful for the help of Johannes Wüthrich who worked on the readout electronics of FACT and always found time to thoughtfully introduce me to the electrical engineering side of things.
Finally, I would like to express my gratitude to the director of the Stefan Meyer Institute, Eberhard Widmann, who gave me the chance to work on this exciting project at the hotspot of particle physics CERN and who always makes sure that the institute is a great place for young students to thrive.

Contents

Introduction

Physics is a never ending journey of describing the nature of our universe. While many phenomena have been examined in great detail more remain to be explored further. Currently, one of the most intriguing subjects in physics is the asymmetry in the amount of matter and antimatter that exists in the world around us. To this day, we have not observed any primordial antimatter and the origin of this imbalance still needs to be investigated. An endeavor that could bring answers to this question is the study of the elusive effect of gravity. The gravitational interaction between matter and antimatter has not been measured with high accuracy and there does not yet exist a complete quantum theory of gravity that describes its properties on an atomic level. Antihydrogen ($\bar{\mathrm{H}}$), being a neutral atom, is a promising candidate not only to study the effect of gravity on an antimatter system but also to perform spectroscopy measurements to compare its internal structure to that of ordinary matter. In both cases any deviation from the properties measured in hydrogen would be a sign of new physics which might contribute to an explanation of the matter-antimatter asymmetry observed today.

In the past, several experiments have tried to measure the acceleration of antimatter in the Earth's gravitational field using charged particles [1]. However, gravity is very weak compared to the electro-magnetic interaction and the uncertainties introduced by the inevitable acceleration due to electric and magnetic stray fields could not be eliminated. Nowadays, twenty years after the first antihydrogen atom ($\bar{\mathrm{H}}$) was produced, the field of antimatter research has developed to a point where precision measurements become possible. The *AEgIS experiment (Antimatter Experiment: Gravity, Interferometry, Spectroscopy)* [2] at the Antiproton Decelerator at CERN aims to

characterize the effect of gravity between matter and antimatter using electrically neutral $\bar{H}$. Neutral particles are less influenced by static fields which is a major advantage compared to previous experiments. Nevertheless, $\bar{H}$ has a magnetic moment and therefore it is still susceptible to gradients of the magnetic field. In order to study the properties of individual atoms related to the faint gravitational force, it is important to have paramount control of all the parameters that might affect antihydrogen. Therefore, measures to minimize electromagnetic field gradients are crucial to make such an experiment possible.
Furthermore, a key part of the AEgIS experiment is the antihydrogen detector. The *Fast Annihilation Cryogenic Tracking detector (FACT)* is a scintillating fiber detector that is specifically designed to detect the production of antihydrogen [3]. An excellent understanding of the detector is key to a successful measurement of $\bar{H}$. Therefore, most of this work deals with the characterization of the signal produced by the silicon photomultipliers in FACT in order to assess the best configuration for an optimized signal-to-noise ratio for $\bar{H}$ detection.
During the initial part of this project I explored different ways to minimize the influence of the magnetic field to be prepared for a successful detection of antihydrogen, this is reported in section 1.3 of this work. The main part of the project is dedicated to the characterization of the FACT detector.

In the **first chapter** the goals and the experimental concepts of the AEgIS experiment are introduced in order to show the role of FACT in the detection of antihydrogen. Moreover, a method to minimize the magnetic field gradients within the AEgIS apparatus is presented.
Chapter two contains an extensive documentation of the FACT scintillating fiber detector and all its components.
Finally, **chapter three** presents an extensive characterization of the silicon photomultipliers used in the detector together with a discussion on calibrating FACT for antihydrogen detection. A concluding summary closes this thesis in **chapter four** while the **appendix** serves as a pool for additional documentation.

Chapter 1

The AEgIS Experiment

This chapter contains an overview of the theoretical considerations that have led to the design of the AEgIS experiment as well as a brief technical description of the apparatus in order to understand the role of and the requirements for the FACT detector. Moreover, a method of minimizing the influence of the magnetic fields on antihydrogen atoms within the AEgIS apparatus is presented.

1.1 Motivation

In general, modern theories of physics are built around symmetries of nature at a fundamental level. These symmetries describe a physical property that remains constant even though the entire system is changed by a corresponding transformation. The symmetry with respect to charge conjugation (C) states that all physical phenomena of our universe are preserved when all particles are replaced by their respective antiparticles. Similarly, our universe should be indistinguishable from one that is either mirrored along all three axis (P-symmetry) or one with time (T) running in the opposite direction. However, these three symmetries all have shown to be violated. In the context of this thesis the violation of the C- and CP-symmetry is of particular importance. According to the Sakharov criteria the violation of those two symmetries are required to arrive at the large imbalance in the amount of

matter and antimatter in our universe that we observe today. The sum of all known CP violations are too small to explain the asymmetry observed today. This contradiction is what motivates to further look for tiny differences in the fundamental properties and to explore whether forces act on matter and antimatter differently. To this day all evidence suggests that fundamental properties of antimatter compared to ordinary matter are either the same or merely of opposite sign. Gravity is the only force whose effect on antimatter still has not been measured with high precision and which still lacks a unification with quantum theory to form a complete quantum theory of gravity. Within such a theory the quantization of spacetime could cause CPT-violating processes that lead to the excess of matter we see today. Nevertheless, the combined CPT-transformation has never been observed to be violated and is a cornerstone of the Standard Model of Particle Physics.
Furthermore, the measurement of the gravitational force is also a test of General Relativity on antimatter. In general, the strength of the gravitational force is determined by the gravitational mass of the object. However, there is a second concept of mass which in theory can deviate from the gravitational mass. This is the inertial mass that determines the reluctance of an object to a change in its motion. General Relativity is built around the observation that both the inertial mass and the gravitational mass of an object are the same. This is called the equivalence principle. An experiment that measures the gravitational acceleration of antimatter and compares it to its inertia, can test this principle on an antimatter system.

1.2 Experimental concept

The AEgIS experiment is located at the Antiproton Decelerator (AD) at CERN which provides bunches of up to 10^7 antiprotons ($\bar{p}$) with a kinetic energy of 5.3 MeV approximately every 100 s. These antiprotons are combined with positrons (e^+) to produce antihydrogen. Currently, most of the experiments at the AD directly mix $\bar{p}$ with e^+ so that antihydrogen is formed in a 3-body recombination where the binding energy of the $\bar{H}$ is transferred to a third positron in the vicinity. In contrast, in AEgIS the positrons are

first converted to positronium (Ps), a bound state of $e^+ - e^-$, before they are combined with $\bar{p}$ [2]. Although this approach might require more effort to implement, it offers several advantages:

(1) First, the cross section for the combination of Ps and $\bar{p}$ to form $\bar{H}$ is proportional to the fourth power of the principle quantum number of positronium: $\sigma_{\bar{H}} = a_0 n_{Ps}^4$. Here a_0 is the Bohr radius and n_{Ps} is the principle quantum number of positronium. Excited Ps can therefore significantly enhance the production rate of antihydrogen.

(2) Second, antihydrogen is created within a narrow range of Rydberg states closely related to n_{Ps}. Rydberg excited $\bar{H}$ is susceptible to inhomogeneous electric fields which makes it possible to form a beam with a precisely controlled electric field gradient. With the sharply defined distribution of states it is easier to predict the electric fields that are required for $\bar{H}$ manipulation and thus makes it less difficult to implement the formation of a beam. For the gravity measurement a horizontal beam will be used to measure the acceleration toward the Earth along the flight path.

(3) Finally, in contrast to the 3-body recombination in which the $\bar{p}$ has to be shuttled into the electrons and therefore always has some additional kinetic energy, by using positronium the antiprotons can be cooled down and kept as stationary as possible during the interaction with Ps. Since the temperature of the antihydrogen that is produced is dominantly governed by the temperature of the antiprotons, in this way colder antihydrogen can be produced. The final temperature of the $\bar{H}$ is a key factor for the success of the experiment, because a lower temperature implies a smaller velocity of the $\bar{H}$ along the gravity module and thus allows more time for the atoms to be accelerated by gravity which leads to a stronger deviation of their trajectories.

The antiprotons delivered by the AD have an energy of several MeV which corresponds to a temperature of $\sim 10^{10}$ K. The goal of AEgIS is to produce antihydrogen with an energy of meV or smaller than 10 K which requires multiple efforts to reduce the temperature of the antiprotons. In order to cool down the antiprotons, they first pass through several foils that act as

energy degraders. Afterwards, a fraction of antiprotons with an energy of keV is caught with a pulsed electric potential and is contained by the static electric and magnetic potentials inside a Malmberg-Penning trap. There are several stacks of electrodes placed along the bore hole of two superconducting solenoids providing a static magnetic field of up to 5 T and close to 1 T respectively. Figure 1.1 [4] shows the layout of the experiment. Inside the traps, antiprotons are cooled further using electrons. Confined at a high magnetic field charged particles loose energy through synchrotron radiation with a power according to $P \sim m^{-4}$. Therefore, only light particles like electrons are cooled efficiently. When antiprotons and electrons are stored within the same trap they exchange their momentum through Coulomb scattering until they reach thermal equilibrium. Therefore, the traps are pre-loaded with electrons to cool the antiprotons through a process called electron cooling. Simultaneously, positronium is produced by collecting more than 10^7 positrons from a ^{22}Na beta-source and implanting them in a cold porous silica target where $\sim 10^6$ Ps are created. The target is located right above the trap for antiprotons inside the 1 T solenoid where antihydrogen is produced. Positronium is formed in two different spin configurations: With a likelihood of 25 % in the para-positronium singlet and with 75 % in the ortho-positronium triplet state. However, only o-Ps has a sufficiently large lifetime of 142 ns to allow for any further manipulations. After its production the positronium is laser excited into high Rydberg states in order to increase its lifetime as well as the cross section ($\sigma_{\bar{\mathrm{H}}} \propto n_{\mathrm{Ps}}^4$) for antihydrogen formation. However, in the presence of electric and magnetic fields high n-states can be ionized. The ionization limit in the AEgIS setup lies around $n_{\mathrm{Ps}} \sim 20$.

Finally, after both Ps and $\bar{\mathrm{p}}$ have been prepared which can take up to several minutes, antihydrogen is formed in pulses with the start time of $\bar{\mathrm{H}}$ production defined by the laser for Ps excitation. A burst of positronium reaches the cold antiprotons in the trap below and antihydrogen atoms are produced. The FACT detector surrounds the production region and is specifically designed to detect and track the decay products of antihydrogen that are created within the experiment upon annihilation. As soon as cold $\bar{\mathrm{H}}$ atoms are formed

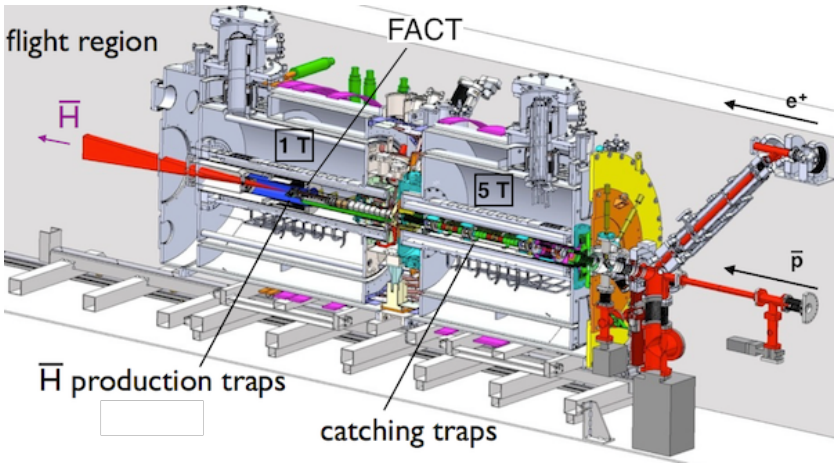

Figure 1.1: *The AEgIS apparatus with antiprotons from the AD entering from the right. The positron accumulation system is connected to the top right and is not shown in this figure. In the center there are two superconducting solenoids with their respective correction coils. To the left inside the 1 T solenoid there is the area of $\bar{H}$ production. The FACT detector surrounds the production trap and the positronium target.*

in large enough quantity, AEgIS will proceed with the measurements on gravity. Since the work on antihydrogen production is still ongoing, the module for the gravity measurement has not yet been installed. Currently, it is planned to form a beam of antihydrogen by applying an electric field gradient which will accelerate half of the $\bar{H}$ (those with appropriate quantum states) towards the detector. This procedure is known as Stark acceleration and has already been demonstrated on hydrogen atoms [5]. Next to the production region there will be an area that is optimized for the gravity measurement so that only small magnetic field gradients are present. In this area along the beam axis a Moiré deflectometer is envisioned followed by a time sensitive antihydrogen detector. The knowledge of the time of production makes it possible to measure a time of flight (TOF) of the $\bar{H}$ atoms. Together with the information on the vertical deflection, the strength of the gravitational force can be determined. This detector concept was successfully tested with antiprotons in the AEgIS apparatus [6]. Additional information on the Moiré deflectometer can be found in [7].

1.3 Optimization of magnetic fields

In preparation for the gravity measurement a study of the magnetic fields within the experiment is necessary. In general, the fields in AEgIS are optimized for the confinement of charged particles. Strong fields up to 5 T are required to achieve the most efficient cooling. The coil system of the 1 T solenoid was designed to mitigate the effect of field gradients towards the gravity module. To measure the effect of gravity the vertical deflection of antihydrogen will be observed. For such a measurement it is important to control gradients both transversally and along the beam axis. Horizontal gradients that are symmetric around the beam axis can have a focussing effect while all other configurations lead to $\bar{\mathrm{H}}$ annihilating on the wall of the apparatus which reduces the overall amount of antihydrogen that is available for experiments. Vertical gradients directly compete with gravity while gradients along the beam axis change the velocity of the atoms between the Moiré gratings and alter the total time that the atom is accelerated by gravity. Both of those components would introduce a systematic error in the gravity measurement.

A simple estimation in equations 1.1 - 1.3 determines the amplitude of the field gradient at which the acceleration by gravity and by magnetic fields are of similar strength. This yields an upper limit of $|\vec{B}'| < 1\,\mu\mathrm{T/mm}$ at a principal quantum number $n = 1$. Higher principal quantum numbers can lead to larger magnetic moments and therefore a stronger effect of the field gradient on the trajectory of the antihydrogen atoms.

$$V = -\vec{\mu}_{\bar{\mathrm{H}}} \cdot \vec{B} = -(g_l m_l + g_s m_s)\mu_B |\vec{B}| \leq n_{\bar{\mathrm{H}}} \mu_B |\vec{B}| \tag{1.1}$$

$$F_g = m_{\bar{\mathrm{H}}} g > n_{\bar{\mathrm{H}}} |\mu| \nabla |\vec{B}| = -\nabla V = F_B \tag{1.2}$$

$$|\vec{B}'| < \frac{1}{n} \cdot 10 \,\frac{\mathrm{Gauss}}{\mathrm{m}} = \frac{1}{n} \cdot 1 \,\frac{\mu\mathrm{T}}{\mathrm{mm}} \tag{1.3}$$

In AEgIS several ways are being explored to achieve this small gradient. One option is the installation of a superconducting Meissner tube enclosing the gravity module. In the bore of a superconducting cylinder the magnetic field

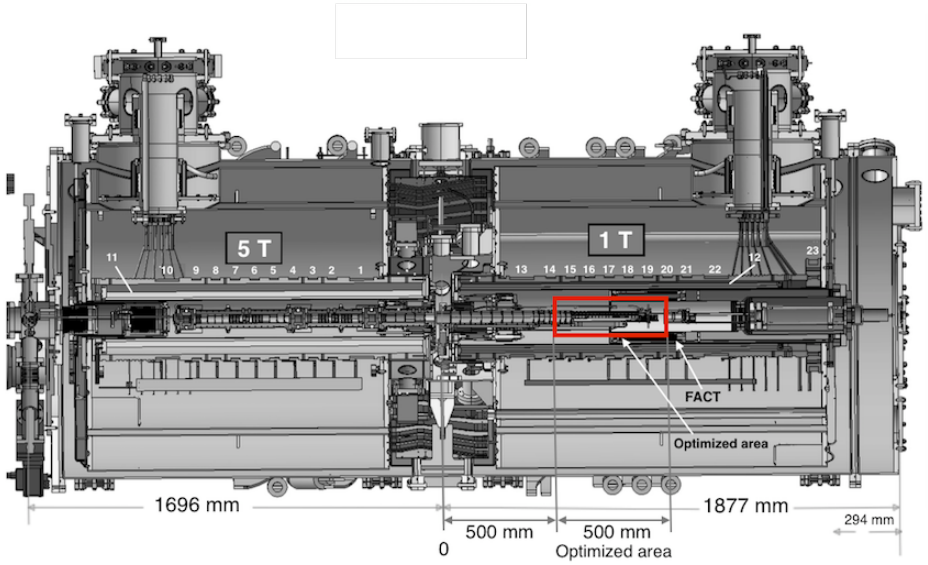

Figure 1.2: *The AEgIS apparatus with the positions of the superconducting coils (1-23) and the area marked in red where the gravity measurement was assumed to take place and where the magnetic field gradients were minimized [9]. The orientation of the experiment with respect to figure 1.1 is reversed. Coils number 11 and 12 are the two main solenoids with a field up to 5 T and 1 T respectively. The FACT detector surrounds part of the optimized region.*

is frozen when it becomes superconducting and the screening currents within the cylinder seek to produce a homogeneous field in its bore. In this way the Meissner tube can act as a shield for magnetic fields and reduce surrounding field gradients. A study on the efficiency of this shields can be found in [8]. A second possibility is to install an active field correction system. Parts of the current system of solenoids can be used as a first element toward this effort. Such a system can always be used to support any additional measures that will be installed in the future. In the following, I describe how the existing setup can be used to actively cancel the largest source of magnetic field gradients which is the fringe field of the 5 T solenoid.

Around the two main solenoids there are 21 cylindrical superconducting correction coils to tune the field in order to achieve homogeneous conditions in the Penning trap. However, they can also be used to reduce magnetic field gradients in the region where the gravity measurement will take place.

In the context of this thesis, the optimal configuration of currents for all of the coils were estimated using semi-analytical equations that are solved with the *Wolfram Mathematica* software. Although the existing setup can only correct gradients along the beam direction due to the coaxial geometry of the coils, an optimization is worthwhile since these gradients are expected to form the largest component. In this simulation the gravity measurement is assumed to take place inside the bore hole of the 1 T trap while the solenoid is used as an additional correction coil (see figure 1.2). The measurement region starts at a distance of 500 mm to the central point between the 5 T and 1 T trap and has a length of 500 mm. All the 12 coils (12-23) that surround this region are solely used to correct for the fringe field of the neighboring 5 T magnet. The currents of the remaining 9 coils in the 5 T region are fixed to established values. More information on the AEgIS solenoids can be found in [10]. In the following the steps to optimize the configuration of currents are explained in detail:

(1) First, the field $B(z, r)$ of each coil is defined analytically using the mathematical model described in [11]. All the solenoids are combined to a global field using the geometry of the system and with the currents of the correction coils as free parameters. From this field the analytic gradient $B'_z(z, r)$ along the direction of the borehole can be calculated.

(2) Afterwards, the horizontal length of the borehole is divided into 10^n points along the center of the trap at which the gradient is evaluated with an initial value of $n = 2$.

(3) The sum of all these gradients is minimized numerically leading to a set of optimal currents.

(4) To test the stability of the solution the number of points that are evaluated is increased by incrementing the variable n from 2 up to $n = 5$ where the computing power limits a further increase. The currents obtained in this way converge to the values given in table 4.1 in the appendix. This method enables a reduction of the field gradients at the center of the trap along the beam axis within the region enclosed between 500 mm to 1000 mm and leads to a gradient that is up to an order of magnitude smaller than the

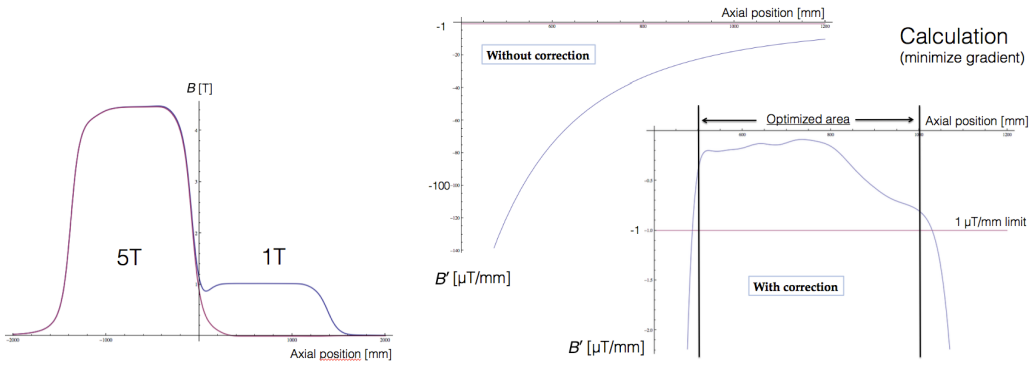

Figure 1.3: *(a) The amplitude of the magnetic field B_z in the direction along the beam axis in the configuration that is used for $\bar{p}$ cooling (blue) or with the set of currents that result in a strong reduction of the magnetic field gradients in the region of the 1 T field (red). (b) The amplitude of the field gradient B_z along the beam axis inside the 1 T solenoid with all the solenoids in the 1 T region (12-23) turned off (top left) and with the gradient-minimizing currents (bottom right).*

requirement of 1 µT/mm for ground state atoms mentioned above. Figure 1.3b shows the field gradient in case all coils around the measurement region are turned off as well as when the optimized set of currents is used.

The approach detailed above is very simple and has a number of limitations. More detailed studies could include the effect of the surrounding components of the AEgIS apparatus and consider their respective material properties which might as well question the cylindrical symmetry that was assumed. However, it is questionable if a more detailed approach yields significantly better results since manual fine-tuning will always be required.

1.4 Antihydrogen detection

The production of $\bar{\mathrm{H}}$ via charge exchange with positronium leads to a pulsed formation. $\bar{\mathrm{H}}$ is electrically neutral and can leave the production trap. Therefore, after antihydrogen is created it drifts toward the surrounding electrodes of the trap and annihilates at wall of the apparatus or with rest gas atoms. As a consequence, the FACT detector cannot measure the annihilation of an-

tihydrogen directly, however it observes the products of its annihilation. The time between production and annihilation will depend on the local quality of the vacuum as well as on the velocity of the antihydrogen that is ultimately determined by its temperature. Furthermore, the decay products of antihydrogen originate from the annihilation of both the antiproton and the positron that together build up the $\bar{H}$. The $\bar{p}$ annihilates with a nucleus of matter producing nuclear fragments and minimum ionizing pions and kaons, while the e^+ annihilates with an electron which produces two photons with a respective energy of 511 keV. FACT is a fiber detector and, therefore, is very inefficient in detecting photons. The range of nuclear fragments is mostly smaller than micrometer and they will not reach the detector. Thus, the only decay products which can be observed by FACT are the charged mesons in the energy range of minimum ionizing particles. Taking into account the geometry of the FACT detector in roughly 75 % of all annihilations only the prongs of two mesons can be detected [12]. Besides the ability to detect pions the design of the AEgIS experiment leads to additional requirements for the FACT detector which are all summarized below.

- **Radial resolution** - The $\bar{H}$ detector should be able to determine whether pions originate from the annihilation of antihydrogen or of trapped antiprotons. The main discriminating feature is the position of the annihilation. $\bar{p}$ are confined by the Penning trap and annihilate with rest gas atoms at the center of the trap while $\bar{H}$ leave the trap and annihilate on the wall of the apparatus. In order to obtain the radial position of the annihilation the detector has to offer the ability to track the flight path of pions in order to reconstruct their vertex.

- **Axial resolution** - For the gravity measurement the antihydrogen will be formed into a beam by inhomogeneous electric fields. To set up and monitor the Stark acceleration a reconstruction of the decay vertices with a spacial resolution along the beam axis is required.

- **Time resolution and rate of events** - The time resolution needs to be large enough to resolve multiple annihilations during a short period

of time. At a temperature of 10 K the peak annihilation rate of $\bar{H}$ happens roughly 18 µs after the formation of antihydrogen at the center of the production trap and after 130 µs, 90 % of $\bar{H}$ have annihilated [13]. Therefore, in case tens of antihydrogen atoms are formed, the recovery or dead time of the detector following a signal needs to be shorter than 500 ns to guarantee a readout efficiency close to 100 %. With an increase in temperature or a higher number of antihydrogen annihilations the rate of events increases and a faster readout is required.
Furthermore, during the production of positronium around 0.4 µs [13] before the formation of $\bar{H}$, a high number of 10^7 photons is produced and will saturate the FACT detector. FACT needs to be ready to detect the antihydrogen that starts to annihilate right after its production so that the recovery time of the detector is required to be shorter than 400 ns.

- **Cryogenic environment** - Since the surrounding superconducting solenoid operates at 4 K the detector has to work perfectly at cryogenic temperatures while releasing a minimum amount of heat with an upper limit of 10 W. Furthermore, the detector will be inside an isolation vacuum of 10^{-6} mbar [3].

- **Radiation environment** - The detector has to be insensitive to the 1 T magnetic field produced by the solenoid. Moreover, it needs to be able to resist a moderate level of radiation throughout its use.

- **Geometry** - There is only limited space available in the cryostat enclosing the production region. The detector has to fit in a cylinder with radius of 68 mm up to 103 mm [3].

Chapter 2

The FACT Detector

Forming antihydrogen is a difficult endeavour. During the initial tests of $\bar{H}$ production in the current geometry of AEgIS only a handful of antihydrogen is expected to be formed in each production cycle. Therefore, the antihydrogen detector should have the highest possible efficiency on the detection of $\bar{H}$ annihilations. Having an effective $\bar{H}$ detector is crucial before the experiment can continue towards a comprehensive measurement of gravity. In the following, the design choices and the technical realization of the FACT detector are explained in detail together with an assessment of the response of the key components of the detector to an antihydrogen annihilation. Finally, a description of the readout electronics completes this chapter.

2.1 Properties

The FACT detector is a barrel-shaped scintillation counter with excellent readout capabilities at cryogenic temperatures. It consists of two active layers around the production region composed of 1 mm *Kuraray SCSF-78M D* multi-clad scintillating fibers[1]. In total 794 scintillating fibers are lined up along the beam axis and are distributed among four sheets so that each layer of the detector consists of two rows of close to 200 fibers. The innermost sheet of fibers of the first layer is placed at a radius of 70 mm followed by

[1]More details on the *Kuraray* fibers can be found in the manual at *http://kuraraypsf.jp/pdf/all.pdf*.

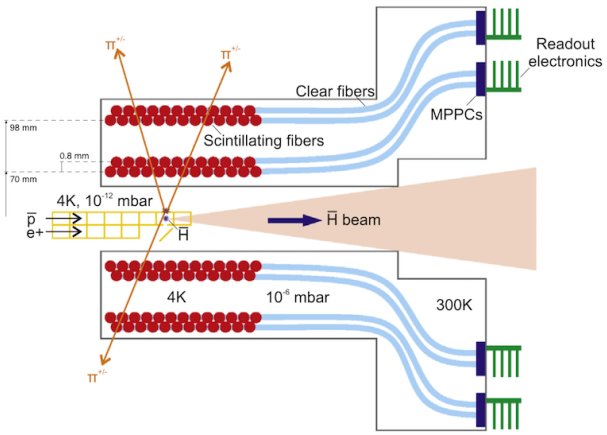

Figure 2.1: *Layout of the FACT detector [3].*

the second sheet at 70.8 mm. The fibers of the second layer have a radius of 98 mm and 98.8 mm. The fibers of one layer are stacked on top of each other with a pitch of 1.2 mm between the individual fibers of each row resulting in a length of the detector of 237.6 mm in the horizontal direction (see figure 2.1). This fine grained layers make is possible to track particles leaving the production area and to obtain information about their vertex. In this way the position of the annihilation along the beam axis can be determined with a resolution of $\sigma_z = 2.1\,\text{mm}$ [3].

2.1.1 Scintillating fibers

In general, scintillation is the emission of photons following the excitation of atoms or molecules by radiation. Therefore, a scintillator converts the energy that a particle deposits inside the scintillator into a light response. The time scale of the de-excitation process to the ground state in an organic scintillator is in the order of ns. More specifically, the *Kuraray* fibers provide a decay time of their light signal of 2.8 ns according to their specification. The cold environment of the production region of 4 K clearly affects the light yield and enhances the decay time of the light signal. However it was shown, that for the fibers used for FACT there is only a small decrease in performance at these temperatures [3].

The frequency of the light produced by a scintillator is independent of the incoming radiation and is distributed according to the emission spectrum of the scintillator material. For the fibers used within FACT the peak emission is in the visible regime at 450 nm. In contrast, the intensity of the light produced from radiation is proportional to the amount of deposited energy which makes it possible to distinguish pions produced by antihydrogen annihilation from other types of particles going through the detector.

In the following, the intensity of light that is produced inside a scintillating fiber that is hit by either a pion or a number of photons is estimated. The amount of photons that can be expected serves as a starting point for the characterization of the photodetector that reads out the scintillating fibers.

First of all (1), the average path of particles through the material of a fiber is calculated. A particle can fly through the center of the fiber but also can hit the edge. The average penetration length can be obtained by integrating all the possible paths through the fiber. In addition, the scintillating core is enclosed by a cladding with a thickness of 8 % of the diameter which has to be excluded so that, overall, the mean path inside the fiber is close to 0.72 mm.

Second (2), the energy deposit of a minimum ionizing particle like the pion with the momentum from an $\bar{\mathrm{H}}$ annihilation within a plastic scintillator is about $2\,\mathrm{MeV\,cm\,g^{-1}}$ [14]. With a density close to $1\,\mathrm{g/cm^3}$ the mean deposited energy is approximately 0.145 MeV which is converted to at least 1000 photons (7000–10 000 photons per MeV [14]). A Monte Carlo simulation for the specific detector geometry shows a similar energy deposit with a mean of $0.199 \pm 0.139\,\mathrm{MeV}$ [15] which corresponds to an average of 1400–2000 photons that are formed inside the scintillating fiber.

Finally (3), only a very small fraction of photons stays inside the fiber. The trapping efficiency for the *Kuraray* fibers is 5.4 %. This means of 1400–2000 photons (0.199 MeV) only 76–108 are trapped within the fiber and guided towards the photo detector. The loss of light along their flight path within the fiber can be neglected since the attenuation length is 387 cm [16] while the length of the fibers in FACT is less than 70 cm. Moreover, to maximize

the light yield the loose end of the fibers is mirror coated with aluminum. However, the interface between the scintillating fiber and the clear fiber as well as the transition between the fiber and the photodetector both introduce additional losses that here can only be estimated.
In a test with ^{90}Sr documented in [17] with a mean energy deposit of 0.19 MeV in the same type of Kuraray fiber but with a length of 2 m a number of 54.5 ± 2.8 photons arrive at the detector. When the photons that are lost by the attenuation along the fiber (40 %) are added, a total of 91 photons would reach the detector. This number is within the estimate of 76–108 photons given above. For this thesis a similar measurement with ^{90}Sr leads to a number of 61^{+24}_{-21} photons reaching the detector. The lower intensity of light might be the result of additional losses on the interface between the fiber and the surface of the readout detector.

A very similar estimate can be done to determine the energy deposit of $e^+ e^-$ annihilations of ortho-positronium to $3\,\gamma$. Since the energy of photons produced by this annihilation is less than 511 keV, the deposited energy within a fiber is much smaller than from a pion. An internal Monte Carlo study [18] shows that the probability of a photon with 500 keV depositing an energy inside the fiber above 200 keV is 0.19 %. Taking into account the subsequent trapping efficiency the number of resulting photons from scintillation is negligible. So any detection of single $e^+ e^-$ annihilations is not feasible. However, during the production and annihilation of bunches of positronium a large number of photons in the order of 10^6 are produced. In this case a substantial amount of energy is deposited inside the fibers and in principle the level of activity over time can be measured.

2.1.2 Muli Pixel Photon Counter

Each of the 794 scintillating fibers is coupled to a clear fiber to transport the signal to a Multi Pixel Photon Counter (MPPC), also called silicon photomultiplier, outside the cryogenic region. With all the readout placed on the outer wall of the experiment there is hardly any heat released inside and there is no space constraint for the readout. In FACT, 766 *Hamamatsu*

S10362-11-100C MPPCs as well as 24 of the more recent model *Hamamatsu S12571-100C* are used. They both consist of an array of 100 individual avalanche photodiodes (APD) covering a total area of $1 \times 1\,\text{mm}$.
A photodiode converts incident radiation to an electric current based on the activation of free charge carriers by the photo effect at the pn-junction of a semiconductor. The resulting electric current can be adjusted by selecting an appropriate operating voltage of the photodiode. In most photomultipliers the applied voltage is selected in such a way so that the resulting current is proportional to the intensity of the incident light. However, an avalanche photodiode is operated in Geiger mode at a reverse voltage that is higher than in the proportional regime and even bigger than the breakdown voltage of the diode. This high electric field inside the semiconductor accelerates any charges induced by external radiation and in this way provides the energy to enable additional electrons to enter the conduction band through impact ionization equivalent to an inverse Auger effect [19]. This process fuels an avalanche that results in a significant electric gain of 10^5–10^6 electron charges [20].
However, this means in principle the magnitude of the electric signal of an individual APD is independent of the intensity of the incident radiation. Regardless of how many photons hit one avalanche photodiode at one point in time it will always produce the same signal depending only on the general operating parameter like voltage and temperature. Therefore, an MPPC consists of multiple APDs so that the number of active diodes can be an indicator of the intensity of the incoming radiation. Moreover, an identical signal is formed in an APD when the original charge is a product of noise instead of actual radiation. Thermal fluctuations can generate free charge carriers that then trigger a dark noise signal. Dark count rates strongly depend on the operating parameter and are different between the two models of MPPCs that are used. At room temperature their dark count rates are specified to be around 600 kHz in the older *S10362-11* and close to 60 kHz in the more modern *S12571* at their recommended operating voltage. The different ways in which MPPCs are affected by noise are characterized in more detail in chapter 3.

At these high levels of amplification within the APD the avalanche current does not cease by itself but to recover the photodiode to its original and sensitive state a quenching resistor is necessary. This resistance is connected in series to the diode and during an avalanche it causes the voltages to drop so that no further charges are created by impact ionization. Therefore, the recovery of the detector signal is purely governed by the design of the quenching resistor and in general is much slower than the initial rise time when the avalanche gets triggered [20]. For both models of MPPCs the rise time is in the order of a few ns while the recovery time is around 200 ns. Still, during the recovery the avalanche can be re-triggered by incident radiation of sufficient intensity, however the gain of the diode is different from its fully recovered state leading to a signal with a modified current and ultimately an output that is harder to interpret.

All the individual avalanche photodiodes of an MPPC are connected in parallel with each APD producing an identical signal when it is hit by at least one photon. In this way all signals are summed up on the output of the MPPC. The amplitude of the final current is multiple times the height of an individual signal and therefore gives the number of activated APDs on an MPPC. At low levels of light where each diode is only hit by up to one photon, MPPCs are an excellent single photon detector. According to the estimation above, up to 108 photons reach the detector when a pion hits a scintillating fiber. Taking into account the photon detection efficiency (PDE) up to 35 % at the recommended operating voltage of both the *Hamamatsu S10362-11-100C* [21] and *S12571-100C* [20], the signal of the photomultipliers can, in an initial estimate, be expected to be close to 36 photons. However, there is a chance that multiple photons hit the same APD. Therefore, a smaller number of photons is registered than the full amount that arrives at the detector. The overall number of APD that gets activated can be calculated with the empirical equation 2.1 taken from [22].

$$N_{fired} = N_{total} \times [1 - \exp(\frac{-N_{photon} \times \mathrm{PDE}}{N_{total}})] \tag{2.1}$$

With the total number of pixels $N_{total} = 100$ and the number of incident

photons $N_{photon} = 108$ the probability of multiple photons hitting the same pixel leads to a small correction resulting in an estimate of up to 31 photons being detected by an MPPC. Still, the interfaces between the fibers and the surface of the detector is not taken into account so that a slightly lower number of photons will be detected.

Nevertheless, the detection efficiency and overall performance of an MPPC is strongly dependent on the operating parameter like temperature and supply voltage which also govern the level of noise that affects the system. An increase in the operating voltage leads to a higher gain as well as a better photon detection efficiency, however it also leads to a substantial increase in the number of noise signals. On the contrary, a rise in temperature reduces the gain of the diodes because it results in an increased collision rate of the charge carriers with the lattice that makes it more difficult to fuel the avalanche. Therefore, it is important to keep the temperature of the MPPCs constant in order to maintain a stable gain and to make a consistent calibration possible. All in all, silicon photomultipliers are a small and efficient alternative compared to the more traditional photomultiplier tubes, especially in big arrays and in combination with a high number of scintillating fibers. Moreover, unlike PMTs they are insensitive to magnetic fields which is an advantage in the given detector environment.

2.1.3 Readout

For each production cycle of antihydrogen the readout of the FACT detector has to be able to process the output of all of the MPPCs during a time period of several hundreds of µs until all the antihydrogen annihilates. In the following, there is a discussion on the design of the readout and of the way in which the large amount of data is reduced to the essential information needed for tracking. Afterwards the experimental realization is described in detail.

First of all, to make sense of the output of the MPPCs they have to be read out at a sufficient rate and resolution. The MPPCs have a response time of a few ns and a recovery time of around 200 ns during which their

current output slowly declines. This signal is fast enough to distinguish signals from consecutive annihilations within one photomultiplier as long as the temperature and the number of antihydrogen atoms stay at the expected values. However, individual annihilation products cross the layers of the detector within a few ns and the readout needs to be fast enough to be able to combine those signals to a track. Therefore, to group signals of both layers produced by the same particle, in FACT all of the 766 *Hamamatsu S10362-11* MPPCs are sampled at a rate of 200 MHz (5 ns). However, at this rate the order in which the fibers are activated and therefore the direction in which the particle goes through the detector cannot be resolved. The remaining 24 *Hamamatsu S12571-100C* are read out at a higher rate of up to 1 GHz in order to offer a more detailed picture in a subset of fibers that is evenly distributed across the detector. Each ADP produces a signal of 10^5–10^6 elementary charges that are released when an avalanche is triggered with the exact value depending very much on the operating parameter of the MPPC (see chapter 3). In FACT this current is amplified and converted to a signal with a peak in the order of a few mV.

The large number of individual detector channels makes it impractical to save the analog output of each MPPC and their response has to be reduced to the essential information required for the vertex reconstruction. What is needed most is the information on whether a fiber is idle or active at any given point in time. To separate the active and the idle state a voltage threshold is introduced. The MPPC is in the *ON* state when it produces an output above the threshold and is recorded to be in the *OFF* state when there is no signal or an output below the threshold. Ideally the limit is set to a threshold voltage that is just below the one that is expected to be created by an actual annihilation product hitting a fiber. With this filter, noise signals of individual APDs of an MPPC can be excluded while all signals from radiation still get recorded. However, there are variations between the MPPCs and each of them has a slightly different gain and noise level when they are operated at the same voltage. Therefore, it must be possible to control the bias and the threshold connected to each MPPC individually to adjust them to an optimal and calibrated value.

Additionally, the output of the 24 *Hamamatsu S12571-100C* is recorded entirely without any zero-suppression in order to have the ability to analyze the response of the detector in more detail. There is an overview of all the readout parameters in table 2.1.

	Hamamatsu S10362-11-100C	Hamamatsu S12571-100C
No. of channels	766	24
Readout	discriminated signal	analog signal
Breakdown voltage	∼70 V	∼65 V
Photo detection eff.	<35 %	<35 %
Recovery time	200 ns	200 ns
Dark Noise	600 kHz	60 kHz
Sampling rate	200 MHz	0.25 GHz/1 GHz

Table 2.1: *Overview of the two MPPC models used within FACT.*

In FACT this readout scheme is implemented as follows[2]: All the scintillating fibers are color coded and organized into 16 bundles of 48 fibers that are each connected to their own readout unit. The readout is placed outside the cryostat to minimize the heat load inside. To guide the light to the readout unit without any additional signals being picked up the scintillating fibers are coupled to clear fibers inside the cryostat and a bundle of 48 clear fibers are connected to 48 MPPCs on a MPPC holder at the back of the AEgIS cryostat. A D-Sub D-50 feedthrough directly connects the photodiodes with an electronic readout box mounted on the outside. Two groups of 48 MPPCs are connected to one box which contains two independent readout modules (see figure 2.2a). For both groups of diodes a backplane fans out the signals to four analog printed circuit boards of 12 channels each. These readout boards control the bias voltage of each MPPC and process their output into a digital signal. A conceptual drawing of the readout can be found in figure 2.2b. A detailed schematic is available in the appendix 4.1. A *Mini-Circuits MAR-6+* amplifier in Darlington configuration with a specified gain of 20 dB amplifies the signal before it reaches a *Analog Devices ADCMP601* comparator that compares it to a threshold voltage and produces a 3.3 V TTL

[2]Additional information on the circuit boards of the readout can be found at *https://twiki.cern.ch/twiki/bin/view/AEGIS/FACTHardware*.

digital output. Both the bias voltage and the threshold are controlled by a *Microchip MCP4242-POT* digital potentiometer. The threshold (THR) can be set to 129 discrete values (0-128) which in the current configuration are in the range of 0 mV to 157 mV. Looking at the schematic the precise voltages that is connected to each threshold setting can be found with equation 2.2. In table 4.2 of the appendix a list of threshold voltages can be found.

$$V_{\mathrm{THR}} = V_{\mathrm{CC}} \frac{R_{\mathrm{pot}}}{R_7 + R_{\mathrm{pot}}} = 3.3\,\mathrm{V} \frac{\frac{\mathrm{THR}}{128}\,10\,\mathrm{k\Omega}}{200\,\mathrm{k\Omega} + \frac{\mathrm{THR}}{128}\,10\,\mathrm{k\Omega}} \tag{2.2}$$

The bias can be selected among 70 discrete values covering a range of about 1.2 V typically between 69.9 V to 71.1 V for the *Hamamatsu S10362-11* and 65.6 V to 66.8 V for the *Hamamatsu S12571*. However, the range can be modified by adjusting the external supply voltage and shows deviations of 0.2 V between different readout channels[3]. Note that in the course of the test done for this thesis it was discovered that the boxes are prone to ground loops that can interfere with the readout.

The settings of the digital potentiometer are controlled by a *Xilinx Spartan 6 SP601* Field Programmable Gate Array (FPGA) numbered 0–15 each associated with one of the 16 bundles of scintillating fibers. The FPGAs regulate the bias and threshold settings, read out the digital output of the comparator and record the changes in the state of the fibers with a sampling rate of 200 MHz. In principle, all the FPGAs operate as independent units, however they are connected via ethernet to a common control server that coordinates the readout and transfers the data from the FPGA to the global data acquisition. Furthermore, each FPGA has a separate trigger input to link it to the global AEgIS experiment with the purpose to synchronize the start of the data acquisition with the procedure to create antihydrogen. Finally, all the FPGAs have to run on a common clock so that the signals from different FPGAs can be combined for tracking. Especially for measurements that take several ms the errors on their internal clock of 200 MHz ± 50 ppm sum up to deviations of multiple clock cycles. Therefore, an additional FPGA is used

[3] A detailed characterization of the bias voltage of each detector channel can be found at *https://twiki.cern.ch/twiki/bin/view/AEGIS/FACTBiasSaturation*.

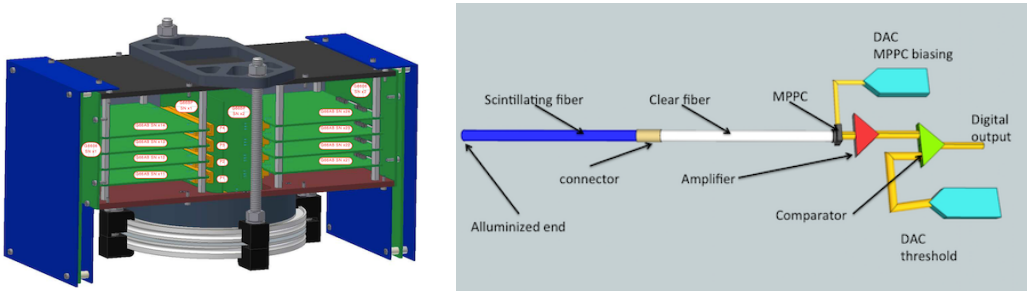

(a) *(b)*

Figure 2.2: *(a) Drawing of the FACT readout box. There are two wings that each record the signal of 48 MPPCs. Each side has four analog readout boards and one FPGA. (b) Structure of the readout starting with the signal of the scintillating fiber to the MPPC and ending with the TTL output that enters the FPGA [3].*

to generate a master clock of 10 MHz that is used as an external reference on the SMA input of each FPGA to correct their internal clock and synchronize the data taking. Each readout box is powered by two power supplies that provide the 6 V supply voltage for the FPGAs and either 84.1 or 90.5 V to supply the bias voltage of the *S12571* and the *S10362-11* MPPC model.

In addition to the readout described above, fibers evenly distributed throughout the layers are connected to a separate analog readout box that directs the amplified signal to a digitizer instead of being processed by the comparator and the FPGAs. There are three digitizers that are used: two *CAEN V1720 - 8 Channel 12 bit 250 MS/s* and a faster *CAEN V1751 - 8 Channel 10 bit 1 GS/s* Digitizer. To read out the fibers of these channels the more recent MPPC model *Hamamatsu S12571-100C* is used. With a total of 28 fibers connected to this additional readout and 24 of them linked to one of the digitizers it leaves two FPGAs with only 47 fibers connected.

2.1.4 Temperature control

Ideally, each MPPC has its own temperature control. However, with hundreds of MPPCs this is a considerable effort. In FACT there is one *PT100* temperature sensor on each MPPC holder of 48 photodiodes that gives the average temperature of those diodes. This value is used in a PID controller to

adjust the power consumption of a ventilator that is mounted on the outside of the readout box. The MPPC holder and the readout box form a heat link so that ultimately the MPPC are kept at room temperature. This is far from perfect, however in this way temperature fluctuations can mostly be reduced to below 0.5 K. The implications of these changes in temperature in regard to a consistent calibration are discussed below.

Chapter 3

Characterization and calibration

A fundamental understanding of the detector response is the basis to finding a calibration of FACT that maximizes the detection efficiency for antihydrogen annihilations. To achieve the best results, the detector has to be configured in a way to detect as many annihilation products as possible while still being able to combine these signals to reconstruct the vertices of antihydrogen atoms. Therefore, the sensitivity has to be balanced with the level of noise that interferes with the precise reconstruction. In this chapter, the silicon photomultipliers that form the read-out system of the FACT detector are characterized and the efforts toward an optimized signal-to-noise ratio are documented. In FACT, the bias voltage of the MPPCs as well as the signal threshold that separates the active from the idle state can both be used to adjust the detector response. To pin down the influence of bias and threshold, a signal with an energy deposit that is similar to the one that is expected as a result of $\bar{\mathrm{H}}$ annihilations is produced in a test setup and the level of noise of the MPPCs and the efficiency toward antihydrogen events are measured.

3.1 Test setup

The entire chain of detection in FACT was reproduced in a tabletop test setup that is shown in figure 3.1a. A light-tight stainless steel chamber houses up to three *Kuraray SCSF-78MD* scintillating fibers with a length of 50 cm that can be connected to either a *Hamamatsu S10362-11-100C* or a *Hamamatsu S12571-100C* MPPC mounted on a MPPC holder on the lid of the chamber (see figure 3.1b). The loose ends of the fibers are mirror coated like in the FACT setup. The scintillating fibers are held in place by an aluminum block with a slit that leaves an area of about 10 mm^2 of the fibers exposed to a Sr-90 beta source and allows multiple fibers to be stacked on top of each other for coincidence measurements. The collimator of the source with a diameter of 7 mm is at a distance of 1 cm above the fibers.

This configuration is similar to the one in [17] where simulations showed that the radiation of the beta minus decay of the ^{90}Sr–^{90}Y mother/daughter pair to ^{90}Zr with a Q value of 2278.5 keV deposits a mean energy of 0.19 MeV in the same type of scintillating fibers. Therefore, a similar energy deposit can be expected here, which is comparable to the energy deposit in the fibers ($\sim$0.2 MeV) by minimum ionizing pions [15]. The source used in the test setup has a specified activity of approximately 31 kBq at the exit of the collimator which results in a rate of up to 2000 Hz at the exposed surface of the scintillator. In addition to the fibers, there is a plastic scintillator with the approximate dimensions of $1\,(h) \times 3\,(w) \times 4\,(l)\,cm^3$ placed below the slit of the aluminum block that in some tests is used as a trigger to distinguish the signals formed by radiation from the noise background. However, only a small fraction of the beta particles has sufficient energy to produce a signal in this additional scintillator after having passed a scintillating fiber previously so that a rate of less than 10 Hz is detected in this configuration.

The MPPCs are read out by the same readout box that is used to connect the photomultipliers with the digitizers in the actual FACT setup and thus offers access to the output of the MPPC both before but also after being processed by the comparator. The output is analyzed with an *LeCroy WavePro 735Zi 3.5 GHz* oscilloscope while the processed signal is saved by the FPGA that is

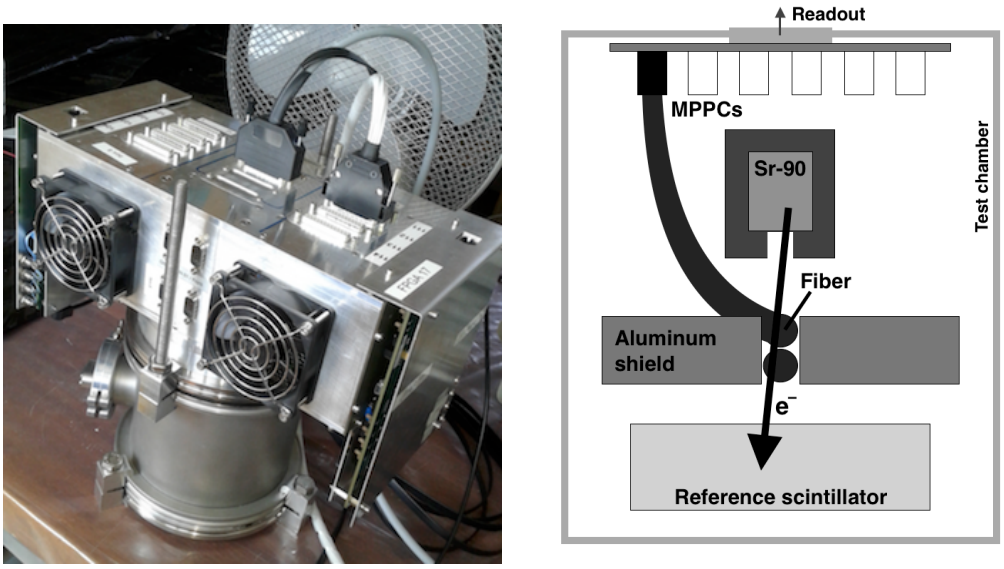

(a) *(b)*

Figure 3.1: *(a) One of the FACT readout boxes connected to the test chamber. In addition to the signal being processed by the comparator, this box provides access to the analog signal via connectors at the top so that is can be read out by the digitizers or the oscilloscope. (b) A sketch of the test setup. Up to three scintillating fibers are held in place by an aluminum holder above which a Sr-90 source is placed. A reference scintillator can be used to trigger the data acquisition.*

part of the readout box. Unfortunately, the trigger rate of the oscilloscope is limited to slightly above 200 Hz depending on the trigger settings so that it is not possible to observe all the signals produced by a MPPC. Moreover, the connection of the oscilloscope to the readout channel leads to reflections along the measurement cable when the line is terminated at 1 MΩ. To obtain a signal shape that resembles the undisturbed signal, the line to the oscilloscope has to be terminated at 50 Ω which leads to measured voltages of half the amplitude of the signal measured at 1 MΩ. This has to be taken into account when looking at some of the figures throughout this chapter. Finally, a *PT100* temperature sensor is mounted next to the photodiodes on the MPPC holder inside the test chamber. If not denoted otherwise, the data shown in this chapter is taken at room temperature of around 24.4 °C.

3.2 Signal properties

The operating voltage of a silicon photomultiplier determines its overall performance including the detection efficiency of the detector, however, at the same time influences the noise level. In order to identify pions from antihydrogen annihilations in the AEgIS apparatus, the expected amplitude of their signals is of particular importance. It links the bias to the appropriate threshold setting in order to optimize the detection of pions while keeping the level of noise to a minimum. The shape of the signal determined by the recovery time of the MPPCs is independent of the operating voltage (see section 2.1.2) and therefore is not touched in the course of the calibration. In the following section, the change in the amplitude of the analog signal of the MPPC to a shift in bias is characterized with the oscilloscope.

3.2.1 Signal spectrum

The avalanche photodiodes that form a MPPC all produce a signal with an almost identical amplitude when they are activated so that the combined output of numerous APDs is restricted to be a multiple of their signal. Figure 3.2 shows a histogram of the peak amplitudes of the signals produced by a *Hamamatsu S12571-100C* MPPC. At small amplitudes it is clearly visible that certain values are more dominant than others. In the histogram each peak corresponds to MPPC signals produced by the same number of active APDs. The amount of active diodes which corresponds to the number of detected photon equivalents (p.e.) is proportional to the intensity of the incoming light so that in figure 3.2 the signal from the Sr-90 source (purple) has a much higher amplitude than pure noise signal (green). With an increase in the number N of active APDs the fluctuations of the combined signal become larger due to small deviations between diodes and variations of the gain due to Shot noise or local inhomogeneities of the detector material. In the histogram this leads to a broadening of the peaks according to FWHM $\sim \sqrt{N}$ [23] so that at high amplitudes the peaks of subsequent photon equivalents overlap each other and cannot be distinguished.
The dark count spectrum in figure 3.2 is the result of two dominant types of

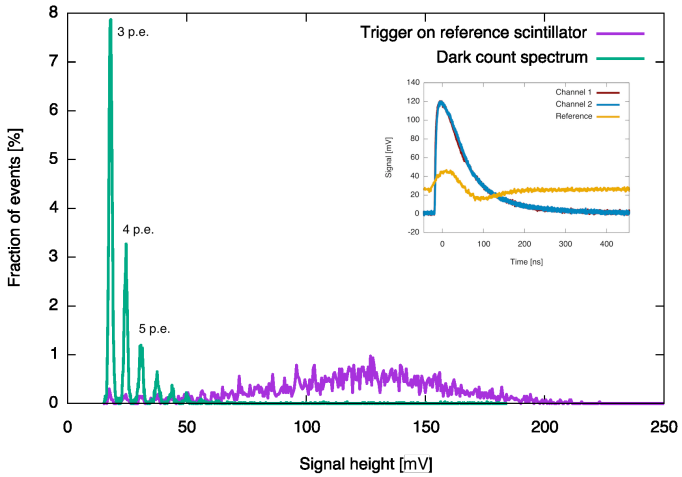

Figure 3.2: *A histogram of the peak amplitudes of signals of a Hamamatsu S12571-100C during the stimulation of the scintillating fibers by a Sr-90 source (purple) and when measuring dark noise (green) collected with 1 MΩ termination. Signals below 15 mV are neglected due to external noise. The operating voltage of the MPPC is 65.48 V (65.47 V recommended). The gain is 6.30 ± 0.11 mV so that the signal from the source is equivalent to 20 ± 6 photon equivalents. The graph in the top right shows the full analog response of two MPPCs (50 Ω termination). The signal from the reference scintillator is used as a trigger.*

noise: A dark count in each APD produced by thermal fluctuations and the propagation of this noise to adjacent avalanche diodes via photons. There are also afterpulses of the initial noise signal that also can be picked up as noise signals but these are explored in a separate section below. The basic noise are individual dark count signals that are triggered by thermal variations which are not correlated and in general only a small number of APDs is triggered simultaneously by this type of noise determined solely by random coincidence. The resulting dark noise, therefore, would be restricted to small amplitudes with up to a few cells that are active. Nevertheless, there is a significant number of noise signals that consist of multiple active APDs which hints to a correlated noise. During the amplification within the diode photons are produced. These photons can travel across the cells and produce a signal in the neighboring APDs which is called optical crosstalk. In this way multiple cells can be triggered virtually at the same time. The extent to which optical crosstalk occurs is proportional to the probability that a

single free charge carrier can trigger an avalanche which in turn depends on the amplification within the diode and thus on the operating voltage. Indicative of the level of crosstalk is the fraction of noise events with an amplitude equivalent to two active APDs compared to the number of events with a single active diode. This crosstalk probability typically is between 10 % to 20 % at the recommended operating voltage. Even though this noise can interfere with the detection of antihydrogen, the noise spectrum can be used to get information about the properties of the detector at a given configuration.

3.2.2 Gain

From noise spectra the gain due to an additional active APD can be obtained at various bias settings by looking at the distance between the peaks in the histogram corresponding to subsequent p.e. signals. In figure 3.3 the results of these measurements are shown. The gain has a linear relation to the operating voltage with an increase of the gain by $3.94 \pm 0.12\,\mathrm{mV/V}$ and $4.92 \pm 0.30\,\mathrm{mV/V}$ for the *S12571-100C* and the *S10362-11-100C* model respectively. However, each MPPC has a slightly different gain at the same operating voltage due to small deviations in the material properties so that the data has to be adapted to their breakdown or their calibrated operating voltage[1]. In general, they are 1 V and 1.4 V above the breakdown voltage for the *S10362-11* and the *S12571* model respectively.
The distance between p.e. pulses can be used to predict the amplitude of a signal of a certain number of active APDs in any bias configuration or vice versa. For example in figure 3.2 the mean peak amplitude of the signals of the Sr-90 source is determined by fitting a gaussian to the spectrum. With a resulting signal height of $124 \pm 36\,\mathrm{mV}$ and a gain of $6.30 \pm 0.11\,\mathrm{mV}$ the signal corresponds to a number of 20 ± 6 photon equivalents. The spread in the number of p.e. is caused by the variations in the number of photons that are created along the different flight paths through the scintillating

[1]The calibrated voltages of the MPPCs within FACT can be found at *https://twiki.cern.ch/twiki/bin/view/AEGIS/FACTMPPC*.

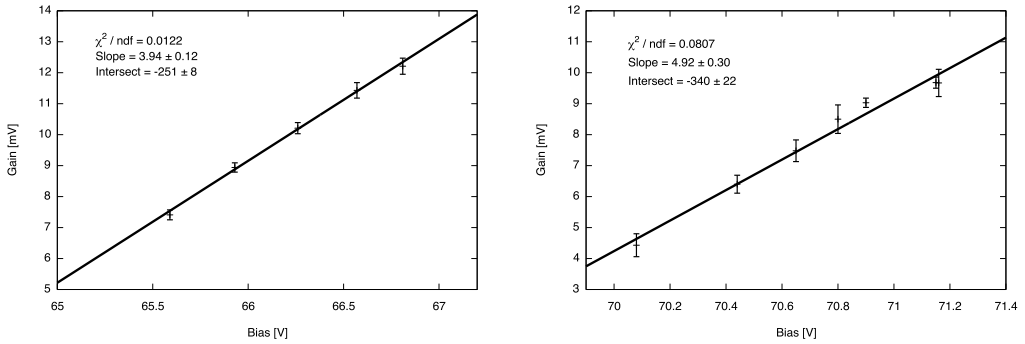

(a) ***(b)***

Figure 3.3: *The mean distance between p.e. pulses at a temperature of 24.4°C (see figure 3.4a) and at various operating voltages of (a) the newer Hamamatsu S12571-100C and (b) the S10362-11-100C. The breakdown voltages are determined by extrapolating the fit and are (a) 63.71 V and (b) 69.10 V.*

fiber as well as the broad energy distribution of the radiation of the Sr-90 source. While for a minimum ionizing pion the energy deposit per mm is more homogenous, the various flight paths through the fiber will still lead to a broadening of the peaks.

Furthermore, the gain is linearly proportional to the temperature of the MPPC in the relevant temperature range which is shown in figure 3.4a. In contrast to the effect of the operating voltage, a rise in temperature increases the collision rate of the free charge carriers within the diode and makes it more difficult for them to obtain enough energy to fuel an avalanche so that ultimately the gain of the diodes is reduced (see section 2.1.2). In FACT, even with an air cooling system to control the temperature using fans (see section 2.1.4) there are fluctuations of $\pm 0.5\,\mathrm{K}$ during one shift of 8 h that lead to changes in the gain of $\pm 0.14\,\mathrm{mV}$ which need to be taken into account.

In addition to the gain of the photomultipliers, the photon detection efficiency and thus the number of incoming photons that are converted to p.e. signals determines the amplitude of the output. Figure 3.4b shows the number of avalanche diodes that is activated during the stimulation by Sr-90 at different operating voltages and the respective standard deviation extracted from the respective signal spectra. With this number and the total number of photons that arrive at the surface of the detector a PDE can be calculated

with equation 2.1. Unfortunately, the number of incoming photons has not been measured. However, in section 2.1.1 the intensity of the light that is produced inside the scintillating fiber and that reaches the surface of the detector has been estimated to be between 76–108 photons and the experiment in [17] with an almost identical setup measured 91 photons arriving at their detector. With the assumption of 91 photons hitting the detector surface the highest photon detection efficiency that was measured is 21.9 % at an overvoltage of 2.06 V ($V_{\mathrm{op}} = 71.16\,\mathrm{V}$) which differs from the 32 % that were determined in [21] at this overvoltage. This can be the result of a misestimation of the number of photons that reach the surface of the detector but is dominantly caused by an underestimation of the number of photon equivalents that are detected. Indeed, during these measurements a saturation of the amplifier that is part of the readout at an output of 300 mV (1 MΩ termination) was discovered (see figure 3.5). Already at an output voltage of 140 mV ($V_{\mathrm{op}} = \sim 70.6\,\mathrm{V}$) the gain of the amplifier is decreased by more than 12.5 % so that also outputs that are much smaller than 300 mV are also affected. As a consequence of the saturation, the distance between the individual p.e. peaks in the signal spectrum is reduced and more avalanche diodes are active than calculated with the gain obtained from the dark noise spectra at low signal heights. The saturation is explored in more detail the section below.

The combination of the gain fluctuations, the PDE which is not known accurately, the temperature variation as well as the variations within individual MPPCs and the detector channels make it difficult to determine a precise amplitude for each number of incoming photons and for every configuration of the MPPC and a validation measurement is necessary in order to verify the position of the signal spectrum. The initial attempt to implement such a measurement is explained in the following. For the majority of the MPPCs inside FACT there is only limited access to the analog output since their signals is reduced to an ON and OFF state determined by the threshold voltage. However, in principle from a survey of the noise spectrum even from this reduced data the current gain of each MPPC can still be obtained. The ON states can be counted and with a scan of the threshold values they can be

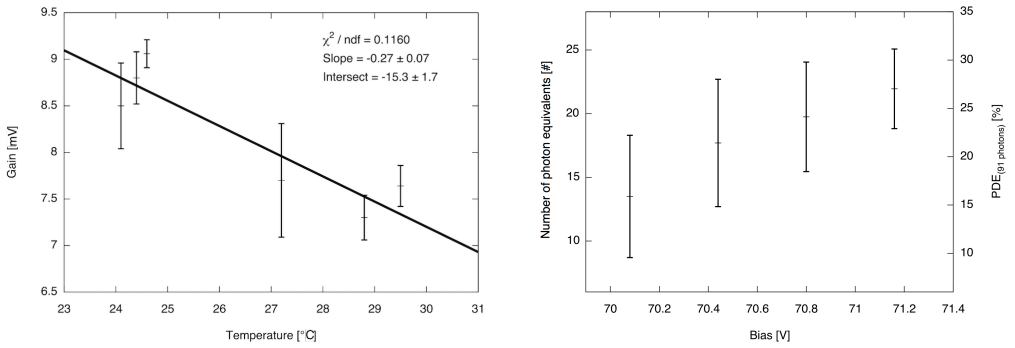

(a) *(b)*

Figure 3.4: *(a) The temperature dependence of the gain of the Hamamatsu S10362-11-100C at an operating voltage of 70.8 V. The temperatures were measured with an uncalibrated PT100 temperature sensor so that only relative temperatures are accurate. (b) The absolute number of p.e. produced in a Hamamatsu S10362-11-100C by the stimulation with Sr-90. Assuming a mean intensity of 91 incoming photons obtained in [17] a PDE was calculated. The number of detected p.e. and thus the PDE is underestimated systematically due to the saturation of the amplifier in the readout. The error bars indicate the standard deviation of the number of p.e. rather than the error of the mean.*

converted to a rate of (noise) signals above a certain amplitude. The result is a step function shown in figure 3.5 with an interval that corresponds to the current gain of the system.

Quite some effort was put into establishing an algorithm that can extract the gain from this noise data of all the MPPCs in FACT, however the discrete threshold settings that can be set with the potentiometer (table 4.2) turned out be too coarse so that the interval could not be resolve consistently. Therefore, the estimate on the expected amplitude of the signals from anti-hydrogen annihilation can only serve as a starting point for an alternative method of calibration.

3.2.3 Amplifier

In the course of the study of the characteristics of the MPPC, a saturation of the amplitudes of the signals was observed. To verify the origin of this saturation and to explore the limitations of the readout a *AIM-TTi TG5011*

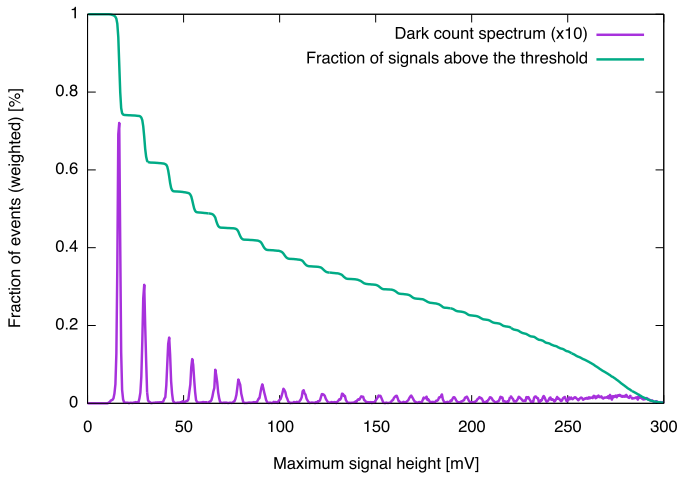

Figure 3.5: *The dark count spectrum of a Hamamatsu S12571-100C MPPC operated with 66.81 V (purple) measured with a termination of 1 MΩ and the fraction of counts with an amplitude above a certain signal height (green). The saturation at an amplitude of 300 mV is visible.*

pulse generator is connected to the input of a readout channel in place of a MPPC. Rectangular test pulses with different amplitudes and widths are sent into the system and the response function of the readout system is measured with the oscilloscope. The figures in 3.6 show the output after the readout. The measurement confirms the saturation of the output at an amplitude of 300 mV (1 MΩ termination) and shows that this feature is produced by the *Mini-Circuits MAR-6+* amplifier of the readout system and not by the MPPCs. Towards this saturation voltage, the spectrum of the MPPC gets more and more compressed at high voltages so that the gain through additional activated avalanche diodes is reduced (see also figure 3.5). While typical signals with 10–25 active APDs as shown in figure 3.4b will be in the range of 50 mV to 220 mV the effect of the saturation occurs there already. An input signal of 10 mV is amplified to 80 mV which is an amplification factor of 8, while an input signal of 20 mV results in an output of 140 mV and an amplification factor of 7 which corresponds to a 12.5 % loss of gain between those output levels. When looking at amplitudes closer to the saturation at an output of 220 mV the amplification factor is

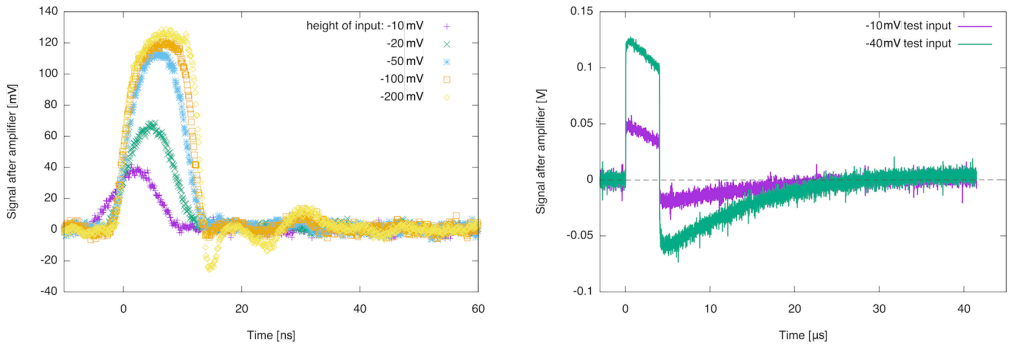

(a) *(b)*

Figure 3.6: *The analog output of an individual readout channel at 50 Ω termination when a square shaped test signal with a given peak amplitude from a pulse generator simulates an idealized signal from a MPPC. Due to the limited capability of the amplifier the signal starts to saturate (a) above an output of 200 mV (converted to 1 MΩ termination) and exhibits an undershoot (b) for long inputs beyond 1 µs even at small amplitudes of 10 mV. The test input is a unit pulse with a FWHM of 5 ns (a) and of 4 µs (b).*

reduced down to 4.4 which is a loss of gain of 45 % compared to the level at 80 mV. Additional corrections are necessary to determine the number of photon equivalents when the signal extends into the saturated region.

Another feature that can be observed during the operation of FACT in the AEgIS apparatus is an undershoot that follows an extended activation of a MPPC of more than 1 µs. When a large number of antiprotons annihilates over the period of several microseconds such signals can occur and might limit the detection of antihydrogen annihilations during the subsequent recovery. In figure 3.6b such an undershoot is reproduced by a 4 µs test pulse. During the production of antihydrogen an undershoot that in some cases can last several tens of microseconds needs to be avoided.

In addition to the specific limitations of the readout, it was discovered that the readout boxes are prone to ground loops when they are connected to several grounds at the same time or when they are not tightened carefully after they have been opened. Furthermore, the readout channels of an entire readout box become unstable when a comparator is set to thresholds below a threshold setting of 15. Then, the noise within the measurement circuit

brings the comparator to oscillate between the active state with a TTL output of 3.3 V and an idle state. The individual readout channels are not well enough isolated so that an oscillation in one channel gets all other channels on the same readout module and even the second readout module within the same box to oscillate as well. Therefore, the threshold can never be set below 19.2 mV or these threshold oscillations will occur and make any measurements impossible.

3.2.4 Afterpulses

When an avalanche is triggered in a photodiode of an MPPCs the free charge carriers can be trapped by inhomogeneities like lattice defects in the amplification region. At the moment they are released they can prompt a new avalanche and a signal that is identical to thermal noise is produced. These secondary signals can occur within a few ns but also up to several ms after the initial pulse. The probability for afterpulses to occur is governed by the overvoltage at which the MPPC is operated. Similar to the way the operating voltage affects the generation of crosstalk it is easier for free charge carriers to initiate an avalanche when there are high fields in the avalanche region of the diode.
Figure 3.7a shows pulses of a *Hamamatsu S10362-11-100C* MPPC at various operating voltages which clearly show the significant increase of afterpulsing at a high overvoltage. In contrast to thermal noise and optical crosstalk, afterpulses often occur during the recovery from the initial event so that the base of the afterpulses is already at a considerable amplitude. Therefore, those pulses tend to have a similar amplitude than the initial pulse which makes it more difficult to distinguish them from actual signals. In FACT, for the majority of MPPCs the signals are selected with a discriminator according to a voltage threshold and there is no direct access to the analog signal which could be used to identify and filter afterpulses. While a threshold can be used to filter the majority of dark count signals, it cannot exclude afterpulses that reach a similar amplitude as the signal pulse with the same efficiency. Every signal pulse can be followed by several afterpulses that

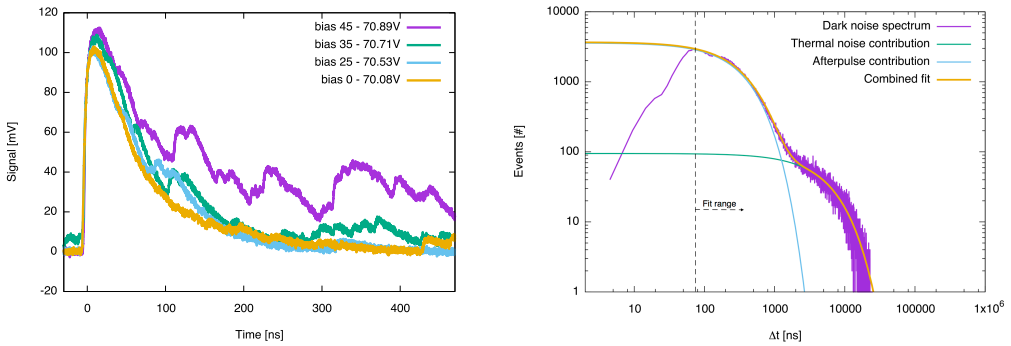

(a) *(b)*

Figure 3.7: *(a) Signals of a Hamamatsu S10362-11-100C MPPC operated with a supply voltage of 90.5 V at various bias settings (breakdown voltage of 69.1 V). (b) A histogram of the time Δt between events with an amplitude above the threshold value of 15 recorded by the FPGA. The MPPC is operated at 71.3 V. The distribution can be described with a combined fit (orange) of two exponentials with different time constants which represent the contribution of thermal noise (green) and of afterpulses (blue) to the total number of noise signals.*

again rise above the threshold and therefore are recorded as separate events. In addition, afterpulses increase the pulse recovery time so that subsequent signals might get lost. Therefore, to optimize the detection efficiency for antihydrogen annihilations it is paramount to understand the contribution of afterpulses and reduce them to a moderate level.

In order to determine the probability for afterpulses to occur at various bias settings and above different thresholds the time gap Δt between consecutive dark count signals is obtained from the discriminated signal recorded by the FPGA. The generation of thermal noise and of afterpulses happens with different time constants and thus the contribution of afterpulses can be separated from the remaining dark noise. In both cases the number of events with a time gap of Δt follows an exponential distribution according to equation 3.1 and 3.2 [20, 21].

$$n_{\mathrm{th}}(\Delta t) = A_{\mathrm{th}} \cdot \mathrm{e}^{-\Delta t/\tau_{\mathrm{th}}} \tag{3.1}$$

$$n_{\mathrm{AP}}(\Delta t) = A_{\mathrm{APf}} \cdot \mathrm{e}^{-\Delta t/\tau_{\mathrm{APf}}} \quad (+ \quad A_{\mathrm{APs}} \cdot \mathrm{e}^{-\Delta t/\tau_{\mathrm{APs}}}) \tag{3.2}$$

Depending on the way the charge carriers are trapped, afterpulses can occur

at several different timescales. Therefore, in equation 3.2 the contribution by afterpulses is divided into a fast (APf) and a slow (APs) component to better represent the data, particularly at lower bias settings. A superposition of the two exponential distributions, one for the thermal noise and one for the afterpulses, is fit to the histogram of the time gaps Δt as shown in figure 3.7b. The graph also reveals a sharp decline in the number of events with a time gap Δt below 75 ns. In this region it is difficult to detect afterpulses with the discriminated signal due to several factors: First, the initial pulse has an amplitude that is larger than the discriminator threshold and needs time to recover below the threshold before a second event can be recorded. Second, during the recovery of a MPPC the charge that is released by re-triggering an avalanche is smaller than an activation in the fully recovered state. Therefore, afterpulses close to the initial pulse have amplitudes that are mostly smaller than 1 p.e. which are less likely to cross the discriminator threshold and produce an event. The amplitude of afterpulses during the recovery is governed by the recovery time τ_{rec} of the MPPC. Finally, the sampling rate of the readout is limited to 5 ns so that features that are smaller cannot be resolved. Therefore, at small values of Δt the efficiency for detecting afterpulses is reduced significantly and only the data with Δt larger than 75 ns is used for the fit. Afterwards, the events that are close to the initial pulse are weighted with an exponential function whose time constant corresponds to the recovery time of the MPPC to take into account the reduced efficiency during the recovery: $\xi(\Delta t) = 1 - \mathrm{e}^{-\Delta t/\tau_{\mathrm{rec}}}$ [21] with $\tau_{\mathrm{rec}} = 33$ ns measured in [24]. With the number of thermal and afterpulse events with a certain time gap $n(\Delta t)$ obtained from the fit at various bias and threshold settings, the fraction of afterpulses compared to the total amount of signals is calculated according to equation 3.3:

$$P_{\mathrm{AP}} = \frac{\int_0^\infty \xi \cdot n_{\mathrm{AP}} \, \mathrm{d}\Delta t}{\int_0^\infty \xi \cdot (n_{\mathrm{AP}} + n_{\mathrm{th}}) \, \mathrm{d}\Delta t} \tag{3.3}$$

The results of this analysis are shown in figure 3.8a where the afterpulse probability for several operating voltages of a *Hamamatsu S10362-11-100C* is shown. In general, the probability for afterpulsing rises quadratically with

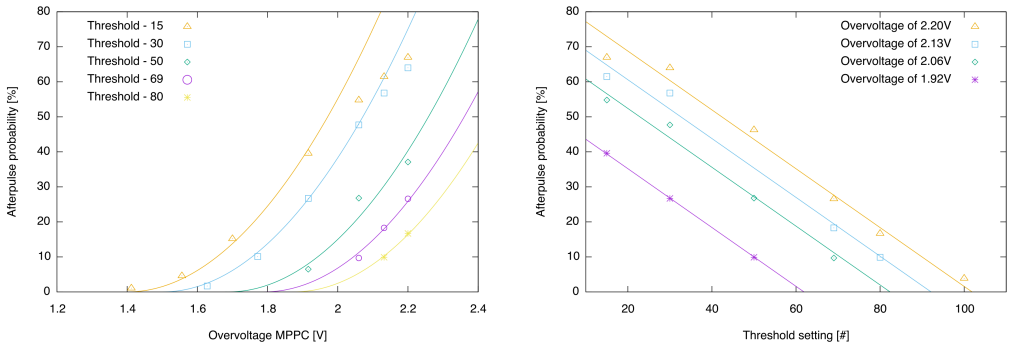

(a) *(b)*

Figure 3.8: *The probability for afterpulses to be detected as a function of the overvoltage (a) and the threshold settings (b) of the S10362-11-100C MPPC. The rise in the probability of afterpulses with an increase of the overvoltage is* $153 \pm 30\,\%/\mathrm{V}^2$. *The fraction of afterpulses decreases linearly with an increase of the threshold setting with* $0.84 \pm 0.06\,\%$ *per threshold step.*

the overvoltage which has been shown in [25]. The average increase obtained from the fit of the data in figure 3.8a is $153 \pm 30\,\%/\mathrm{V}^2$. For these fits, data points with a contribution of afterpulses beyond 50 % are ignored. When the amount of afterpulses is very large the length of the original signals increases dramatically and the probability that an afterpulse occurs before the signal can decrease below the discriminator threshold becomes very high. Therefore, the number of afterpulses that are measured are smaller than the actual amount.
Furthermore, figure 3.8b shows the afterpulse probability for various threshold settings. When the operating voltage is fixed and the threshold setting is increased, the fraction of afterpulses decreases linearly with $0.84 \pm 0.06\,\%$ per threshold setting.

Overall, the threshold setting can be used to filter afterpulses quite efficiently in case it is possible to go to high values without sacrificing much signal efficiency. This can be shown to be possible for an overvoltage below 2 V: The stimulation of the scintillating fibers by the Sr-90 source produce a signal of $213 \pm 31\,\mathrm{mV}$ in a *S10362-11-100C* MPPC operated with an overvoltage of 2.06 V. When the threshold is set to three standard deviations below the mean signal at 121 mV (threshold setting of 98) so that 99.7 % of the signals

are detected the afterpulse probability shown in figure 3.8b is negligible. However, the fraction of afterpulses is measured in relation to the number of dark count pulses and thus it is important to also know the overall level of noise. Furthermore, pulses from an antihydrogen signal are generally larger than dark count pulses and with more APDs being active there are more charge carriers that can be trapped so that the probability for afterpulses to occur is increased. Therefore, a signal pulse will be followed by a larger amount of afterpulses than indicated by the afterpulse probability measured on dark noise. Any configurations with a probability for afterpulses above 50 % should be avoided since the output of the MPPC starts being dominated by afterpulses and it is not possible to extract antihydrogen signals reliably.

3.3 Detection efficiency

The study on the signal amplitude that can be expected from the pions from antihydrogen annihilations in the previous section can be used to decide the discriminator threshold and makes the signal threshold a strong tool to improve the signal to noise ratio. However, the rate of events that are observed at those settings has not been measured. In the following, the absolute level of noise and the efficiency for detecting Sr-90 signals are presented for various combinations of bias and threshold settings.

3.3.1 Noise level

With an accurate discriminator threshold a big fraction of noise signals can be excluded. Nevertheless, certain noise events can pass this filter since the noise of the MPPCs can result in outputs that are identical to the signal events. Therefore, in addition to the discrimination based on the intensity, FACT is designed to allow vertex reconstruction. Hits belonging to the same antihydrogen annihilation can be identified by selecting a narrow coincidence time window of one or two clock cycles (corresponding to 5-10 ns). Additionally, any particle that hits a layer of the detector is very likely to produce a signal in two adjacent fibers since the two rows of scintillating fibers overlap.

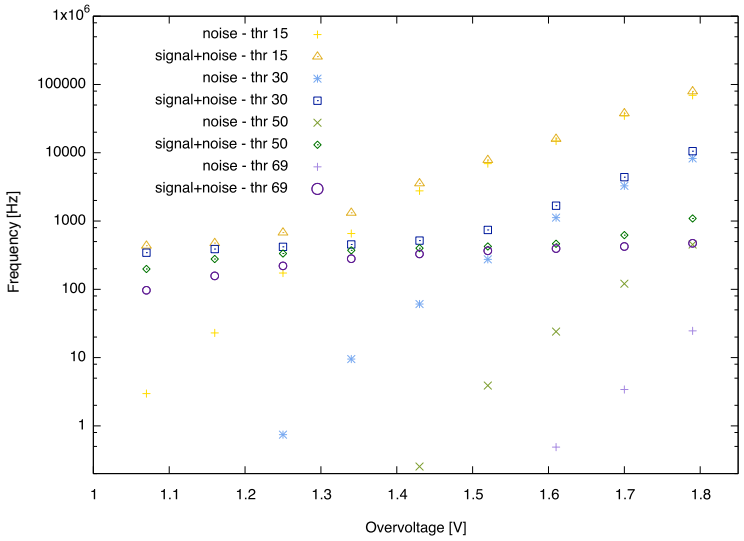

Figure 3.9: *The number of events of a S10362-11-100C MPPC at a given overvoltage and with various discriminator thresholds when pure dark noise is measured and when the scintillating fibers are stimulated by the Sr-90 source.*

To make sure that relevant signals can be selected in this way the probability for a coincidence of noise events above the signal threshold in adjacent detector channels needs to be negligible. This gives a general limit on the maximum level of noise that can be accepted in individual MPPCs which was determined with a Monte Carlo simulation of 766 channels (excluding 28 fibers that are connected to the digitizers) assuming a coincidence when adjacent events occur within two readout samples of 5 ns. This simulation shows that with a level of noise of 1000 Hz in each MPPC, the time during which no coincident noise event occurs in the detector channel of two adjacent fibers with a probability of $3\,\sigma$ is 208 ± 20 µs. Compared to the time of 130 µs during which 90 % of the total number of $\bar{\mathrm{H}}$ at 10 K annihilates [13], the contribution of noise is negligible in the time period during which antihydrogen annihilations can be detected whenever the individual noise levels are kept below 1000 Hz. In case only events with two signal clusters within one coincidence window (one in each layer) are selected, the noise limit can be even higher. This is true unless there is correlated noise between adjacent fibers which was not investigated within this thesis. Figure 3.9 shows the re-

sult of measurements on the pulse rates of a *S10362-11-100C* MPPCs in the test chamber. At four different discriminator threshold the pure dark count rate is compared with the rate of signals that is obtained when the scintillating fiber is stimulated by the Sr-90 source. The results of the measurements taken at a given threshold can be divided in three regions:

(1) At a small overvoltage there is hardly any noise and only the intense signals from the source and a minor amount of afterpulses can exceed the threshold voltage. When the discriminator threshold is increased, some of the signals from the source are below the threshold and, therefore, the number of detected signal is reduced. In principle, by scanning the discriminator threshold at these low operating voltages the mean peak amplitude of the source signal can be determined.

(2) At a slightly higher operating voltage the dark counts start to exceed the threshold and the rate of noise increases exponentially. In this region the dark count rate is still at a moderate level ($<$1000 Hz) while the yield of the source signal shows a small increase. This slight increase is caused by the rise of the gain of the MPPCs which allows signals with a smaller number of p.e. to exceed the discriminator threshold. The extend to which the signal yield is increased depends on the spread of the signal and is more pronounced with the broad spectrum of the Sr-90 source than it will be with minimum ionizing pions.

(3) In case the overvoltage is increased further, the output gets dominated by noise signals. The dark count rate can be reduced with a high discriminator threshold, however in this way the signal yield is also lowered. Moreover, at large operating voltages there is an excess of dark noise in combination with afterpulses so that the photodiodes are firing continuously and in this way affect the signal even though the amplitude of the noise pulses is below the threshold of the discriminator.

3.3.2 Signal yield

From the data in figure 3.9 the number of events that originate from the beta source can be determined. The pure dark noise rate is subtracted from

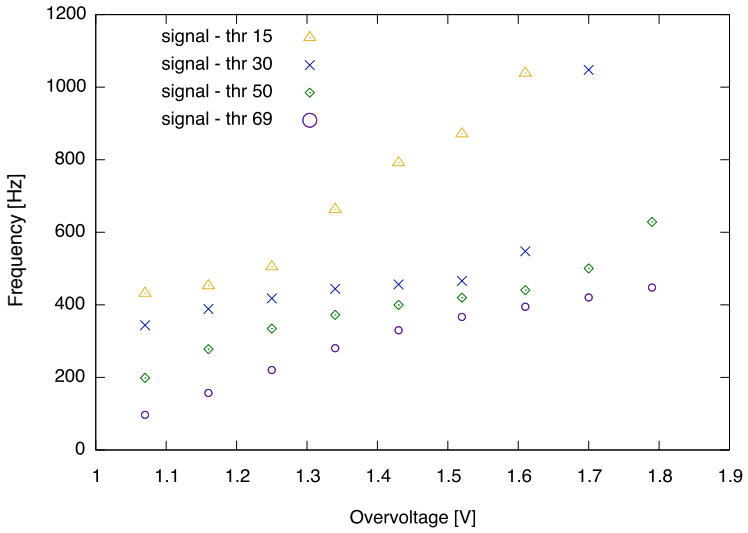

Figure 3.10: *The number of events from a Hamamatsu S10362-11-100C that originates from the Sr-90 source. The rates are corrected for the fraction of afterpulses in the respective dark count spectra using the data in figure 3.8. At all threshold settings the signal rate converges toward a plateau at close to 430 signals before a nonphysical surge that leads to an increase far above the activity of the source. There are indications that this is an artifact of the measurement method.*

the event rate that includes the Sr-90 signals and the resulting number of signals is corrected for the fraction of afterpulses it contains according to the distribution in figure 3.8a. The results are shown in figure 3.10.
With an increase of the overvoltage, first, the signal rate at each discriminator threshold converges toward a plateau at close to 430 signals. With a rise of the gain, signals with a smaller number of p.e. exceed the discriminator threshold up to a point where most of the signals from the source are detected. As a consequence, hardly any additional source signals are detected by a subsequent increase of the operating voltage and a plateau occurs in figure 3.10 at a level that represents the total number of source signals that can be detected by the MPPC. The goal of any calibration should be to get as close to this maximum number of detected signals as possible. Unfortunately, no accurate detection efficiency can be calculated since the total activity of the Sr-90 source at the scintillating fiber is not known. In section 3.1 the intensity of the radiation is estimated to be up to 2000 Hz. However, this activity includes beta radiation with a wide range of energies so that the

number of signals that are formed in the scintillating fiber and which produce a signal in a MPPC may be less than that. Nevertheless, the detection efficiency can be estimated to be more than 21.5 %.
When the operating voltage is increase further, there is a surge in the number of signals that remains even though the dark count noise was subtracted. The origin of the dramatic rise of the measured signal rates at a noise level above ∼1000 Hz is not completely clear. When the measurement time to determine the average noise rate is increased, the sudden rise of the signal rate occurs at a higher overvoltage which hints toward it being an artifact of the measurement method. An additional indicator that this feature cannot represent actual signal events is the fact, that the signal rises well beyond the estimated activity of the source at the scintillating fiber.
After all, this region can be avoided easily without any loss in the detection efficiency since the surge occurs only after the signal plateau has been reached. Then most of the signals from the source are already above the discriminator threshold and therefore not many signals are lost when the operating voltage is kept below this level.

Chapter 4

Summary and Outlook

In this thesis the properties of the Hamamatsu S10362-11-100C MPPC including the gain, the photon detection efficiency (PDE) and the afterpulse probability are documented. Although, it is difficult to predict a precise signal amplitude, the results from studying a Sr-90 reference source can be used to make an estimation on the amplitude of the antihydrogen signals which can serve as a starting point for a calibration of FACT. Furthermore, the measurements of the overall level of dark counts and the afterpulse probability both set upper boundaries for the operating voltages that is connected to a given threshold value. Moreover, the rates of signals from the reference source converges toward a maximum and thus suggests bias and threshold configurations that promise a signal yield close to the maximum value.
Unfortunately, with the AEgIS apparatus closed and the MPPCs installed inside, there is no dedicated reference source to verify and to optimize the signal yield of the MPPCs. In the following months a tracking algorithm will be implemented so that cosmics can be used to optimize the calibration of the detector. Furthermore, the pions from antiproton annihilations can be used as a reference in combination with external scintillators to measure the energy that is distributed among the fibers. The results obtained during this thesis can be used to support any additional measures of optimizing the calibration of FACT toward a successful detection of antihydrogen annihilation this year.

Appendix

Magnetic field configuration

Coil number	Fixed current [A]
1	-10.8
2	5
3	2.5
4	1.4
5	0
6	0
7	-1
8	1.4
9	0
10	10.8
11	150

Coil number	Optimized current [A]
12	-1.24
13	-5.45
14	-3.78
15	-2.76
16	-1.62
17	-0.94
18	-0.43
19	-0.04
20	0.23
21	0.47
22	0.31
23	-0.04

Table 4.1: *Table of correction coil currents optimized within the 1 T main solenoid starting at 500 mm up to 1000 mm from the central point between the main magnets. Currents on the left are fixed values that are currently used in the experiment while on the right are the optimized currents to keep the magnetic field gradient to a minimum.*

Technical Summary

A collection of all the information on the FACT detector can be found in the CERN AEGIS Twiki at: https://twiki.cern.ch/twiki/bin/view/AEGIS/FACT

Threshold setting	Threshold [mV]
1	1.3
5	6.4
10	12.8
15	19.2
20	25.6
25	31.9
30	38.2
35	44.5
40	50.8
45	57.0
50	63.2
55	69.4
60	75.6
65	81.7

Threshold setting	Threshold [mV]
70	87.8
75	93.9
80	100.0
85	106.0
90	112.1
95	118.1
100	124.1
105	130.0
110	136.0
115	141.9
120	147.8
125	153.6
128	157.1

Table 4.2: *A selection of threshold voltages connected to threshold setting of the digital potentiometer calculated with equation 2.2.*

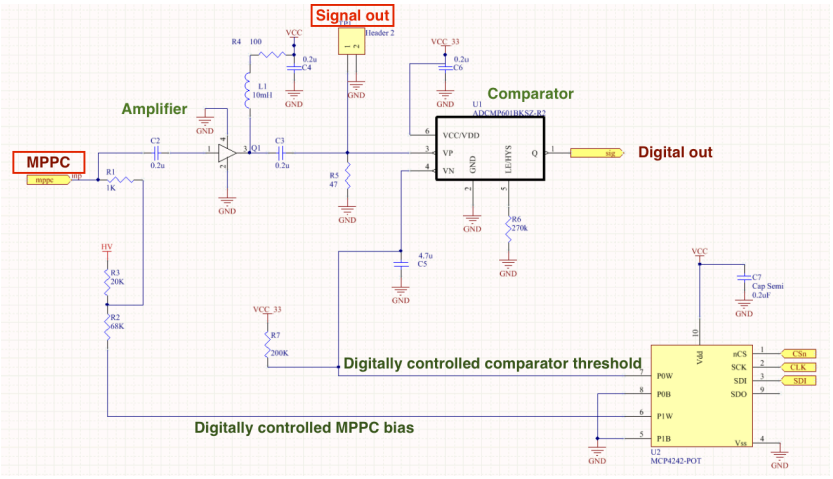

Figure 4.1: *Schematic of the FACT readout. [4]*

List of Figures

Bibliography

[1] T. W. Darling et al. The fall of charged particles under gravity: A study of experimental problems. *Rev. Mod. Phys.*, 64:237–257, 1992. doi: 10.1103/RevModPhys.64.237.

[2] G. Dobrychev et al. Proposal for the AEGIS experiment at the CERN Antiproton Decelerator (Antimatter Experiment: Gravity, Interferometry, Spectroscopy). *CERN-SPSC-2007-017, CERN-SPSC-P-334*, 2007.

[3] J. Storey et al. Particle tracking at 4 K: The Fast Annihilation Cryogenic Tracking (FACT) detector for the AEgIS antimatter gravity experiment. *Nucl. Instr. Meth. Phys. Res. A*, 732:437–441, 2013. ISSN 0168-9002. doi: 10.1016/j.nima.2013.05.130.

[4] J. Storey et al. Particle tracking at cryogenic temperatures. In *Proceedings, 10th International Conference on Position Sensitive Detectors (PSD10)*. JINST, 2015. doi: 10.1088/1748-0221/10/02/C02023. `https://indico.cern.ch/event/174805/contributions/1434396/`.

[5] E. Vliegen and F. Merkt. Stark deceleration of hydrogen atoms. *J. Phys. B*, 39(11):L241–L247, 2006. doi: 10.1088/0953-4075/39/11/L03.

[6] S. Aghion et al. A moiré deflectometer for antimatter. *Nat. Commun.*, 5:4538, 2014. doi: 10.1038/ncomms5538.

[7] Markus K. Oberthaler et al. Inertial sensing with classical atomic beams. *Phys. Rev. A*, 54:3165–3176, 1996. doi: 10.1103/PhysRevA.54.3165.

[8] L. Wéra et al. Magnetic Shielding with Bulk High Temperature Superconductors: Improvement of the Shielded Volume in Hollow Cylinders. In M. Muralidhar, editor, *Superconductivity: Applications Today and Tomorrow*, chapter 5, pages 95–114. Nova Science Publishers New York, 2016.

[9] J. Rochet. The AEgIS apparatus (technical drawings). `https://twiki.cern.ch/twiki/bin/view/AEGIS/AEGISWGThirtyPerc`, AEgIS Collaboration, 2016.

[10] A. Dudarev et al. Construction and test of the magnets for the AEgIS experiment. *IEEE Trans. Appl. Supercond.*, 22(3):4500304–4500304, 2012. ISSN 1051-8223. doi: 10.1109/TASC.2011.2180491.

[11] N. Derby and S. Olbert. Cylindrical magnets and ideal solenoids. *Am. J. Phys.*, 78(3):229–235, 2010. doi: 10.1119/1.3256157.

[12] D. Pagano, G. Bonomi, and N. Zurlo. On the reconstruction of annihilation vertices with the FACT detector. AEgIS Collaboration Meeting, 2017. `https://indico.cern.ch/event/630100/`, Università degli Studi di Brescia & INFN.

[13] Y. Allkofer and J. Storey. AEgIS central detector : Boundary condition & possible technologies. AEgIS Bergen Workshop, 2011. `https://twiki.cern.ch/twiki/bin/view/AEGIS/FACTPresentationsInternal`.

[14] C. Joram, G. Haefeli, and B. Leverington. Scintillating fibre tracking at high luminosity colliders. *J. Instrum.*, 10(8):C08005, 2015. doi: 10.1088/1748-0221/10/08/C08005.

[15] G. Bonomi. Private communication. AEgIS Collaboration, 2017.

[16] A.E. Baulin et al. Attenuation length and spectral response of Kuraray SCSF-78MJ scintillating fibres. *Nucl. Instr. Meth. Phys. Res. A*, 715: 48–55, 2013. ISSN 0168-9002. doi: 10.1016/j.nima.2013.03.027.

[17] T.D. Beattie et al. Light yield of Kuraray SCSF-78MJ scintillating fibers for the gluex barrel calorimeter. *Nucl. Instr. Meth. Phys. Res. A*, 767: 245–251, 2014. ISSN 0168-9002. doi: 10.1016/j.nima.2014.08.038.

[18] G. Nebbia. Monitoring the Ps formation both in the AEgIS setup and in the Ps chamber (technical report). `https://twiki.cern.ch/twiki/bin/view/AEGIS/FACTPositroniumDiagnostics`, AEgIS Collaboration, 2017.

[19] E. Hering, K. Bressler, and J. Gutekunst. *Elektronik für Ingenieure und Naturwissenschaftler*. Springer Berlin Heidelberg, 2017. ISBN 978-3-662-54214-9. doi: 10.1007/978-3-662-54214-9.

[20] A. Ghassemi, K. Sato, and K. Kobayashi. Technical note - mppc. Technical Report KAPD9005E01, Hamamatsu Photonics K.K., 2017.

[21] P. Eckert et al. Characterisation studies of silicon photomultipliers. *Nucl. Instr. Meth. Phys. Res. A*, 620:217–226, 2010. doi: 10.1016/j.nima.2010.03.169.

[22] D. Renker and E. Lorenz. Advances in solid state photon detectors. *J. Instrum.*, 4:04004, 2009. doi: 10.1088/1748-0221/4/04/P04004.

[23] Valentina Arosio et al. An Educational Kit Based on a Modular Silicon Photomultiplier System. In *ANIMMA*, 2013. doi: 10.1109/ANIMMA.2013.6728000.

[24] H. Oide et al. Study of afterpulsing of MPPC with waveform analysis. In *New photon-detectors*. International Workshop on New Photon Detectors (PD07), Kobe University, 2007.

[25] Y. Du and F. Retière. After-pulsing and cross-talk in multi-pixel photon counters. *Nucl. Instr. Meth. Phys. Res. A*, 596(3):396–401, 2008. doi: 10.1016/j.nima.2008.08.130.